Available online at www.sciencedirect.com

SciVerse ScienceDirect

Ceramics International 39 (2013) 7563–7569

CERAMICS INTERNATIONAL

www.elsevier.com/locate/ceramint

Ternary phase relations in CeO_2–$DyO_{1.5}$–ZrO_2 system

V. Grover, A.K. Tyagi*

Chemistry Division, Bhabha Atomic Research Centre, Mumbai 400085, India

Received 29 January 2013; received in revised form 31 January 2013; accepted 2 March 2013
Available online 14 March 2013

Abstract

The present work explores the sub-solidus phase relations in the CeO_2–$DyO_{1.5}$–ZrO_2 ternary system. About 80 compositions in $Zr_{1-x}Dy_xO_{2-x/2}$, $Ce_{1-x}Dy_xO_{2-x/2}$, $(Ce_{0.8}Zr_{0.2})_{1-x}Dy_xO_{2-x/2}$, $Zr_{1-x}(Ce_{0.2}Dy_{0.8})_xO_{2-0.4x}$, $Ce_x(Dy_{0.5}Zr_{0.5})_{1-x}O_{1.75+x/4}$ systems, were synthesized and explored to investigate the phase fields in this ternary system. Detailed XRD analysis showed the existence of a variety of phase fields viz. Fluorite-type cubic, C-type cubic, biphasic fields containing both F-type and C-type phases as well as co-existence of two different fluorite type phases. A few compositions also showed the presence of monoclinic as well the tetragonal phases. The trends observed in cell parameter are found to be governed by the competing factors of average ionic radius and the repulsion between excess anions in the lattice due to the aliovalent substitution. This ternary system showed the existence of a very wide cubic phase field. This ternary phase relation has relevance to the inert matrix fuel concept.

Keywords: A. Calcination; A. Powders: solid state reaction; B. X-ray methods; D. CeO_2; D. ZrO_2

1. Introduction

Inert matrix fuel is a concept proposed for the utilization of large stock of plutonium in uranium-free matrix [1,2]. The concept is also being contemplated for minor actinides transmutation to minimize the volume, quantity, and radio-toxicity of nuclear wastes. In these fuels, an inert matrix serves as a support for the actinide phases, as does the non-fissile $^{238}UO_2$ matrix for PuO_2 in a typical fast breeder MOX fuel. A number of host lattices like multi-phase ceramic–ceramic composites (MCC) based on zirconia, alumina, magnesia [3], as well as several nitrides, carbides [2] and phosphates [4] are being considered to act as an inert matrix, for diluting and utilizing plutonium. A considerable work has also been carried out to assess the stability of these matrices under irradiation [5,6].

An inert matrix fuel should essentially consist of three components (i) host lattice (matrix component), (ii) fissile phase, (iii) burnable poison or a fertile additive. In view of this, CeO_2 (ceria)–Dy_2O_3 (dysprosia)–ZrO_2 (zirconia) system is highly relevant to the inert matrix fuel project. Ceria is used as a surrogate material [7] in place of plutonia (fissile phase). Dysprosia with its high neutron absorption cross section is a burnable poison. Cubic zirconia has been proposed as an attractive actinide host because it is isostructural with the cubic oxide of plutonium (PuO_2) and most of the actinides have large solubility in zirconia. Moreover, rare-earth sesquioxides (Er_2O_3, Dy_2O_3, Gd_2O_3, etc.), proposed as burnable poisons also have large solubility in zirconia [8], which enables loading of an actinide-bearing zirconia waste-form or fuel-form with rare-earths to serve as depletable neutron absorbers. Further, zirconia is highly stable and has got favorable neutronic properties. These properties make zirconia a potential candidate for inert matrix.

Rare-earth doped ceria has also attracted considerable attention as the electrolyte for intermediate temperature solid oxide fuels cells. Several studies have been performed on the pseudo-binary phase diagrams/phase relations in systems like CeO_2–ZrO_2 [9] and CeO_2–Dy_2O_3 [10]. The phase diagram of CeO_2–ZrO_2 system consist of two regions namely monoclinic solid solution up to about 18 mol% of ceria into zirconia and two-phase region consisting of tetragonal solid solution and cubic solid solution. On heating to appropriately higher temperatures, depending upon the composition, the monoclinic and tetragonal solid solutions transform to tetragonal and cubic

*Corresponding author. Tel.: +91 22 559 5330; fax: +91 22 550 5151.
E-mail address: aktyagi@barc.gov.in (A.K. Tyagi).

0272-8842/$ - see front matter © 2013 Elsevier Ltd and Techna Group S.r.l. All rights reserved.
http://dx.doi.org/10.1016/j.ceramint.2013.03.009

solid solutions, respectively. Lee et al. [10] have studied the phase relations and electrical conductivity of solid solutions in CeO_2–Dy_2O_3 system. Similarly, Wang et al. have also studied the synthesis and electrical conduction of 10 mol% Dy_2O_3 doped CeO_2 to reveal the variation of conductivity with grain size [11]. Earlier, the ternary phase relations have been established in various systems like CeO_2–ThO_2–ZrO_2 [12], CeO_2–Gd_2O_3–ZrO_2 [13] and CeO_2–Gd_2O_3–ThO_2 [14] which provided an insight into the different kinds of phase fields that could exist in these systems.

In order to investigate still newer inert matrices, it is required to construct the sub-solidus phase equilibria in the various other systems so as to identify suitable single phasic/multiphasic compositions which might act as inert matrix for hosting Pu or minor actinides (in case of transmutation). It may be noted that the ternary phase diagrams on nuclear materials are not that well reported compared to the binary phase diagrams. In this article, an attempt is being made to unravel the sub-solidus phase relations in CeO_2–Dy_2O_3–ZrO_2, under slow cooled conditions.

2. Materials and methods

The starting materials CeO_2, Dy_2O_3 and ZrO_2 (all 99.9%) were preheated at 900 °C for overnight. The starting materials were well characterized by powder X-ray diffraction for their phase purity. About 80 compositions in CeO_2–Dy_2O_3–ZrO_2 system were synthesized by a three stage heating protocol, as follows: The intimately ground mixtures were heated in the pellet form at 1200 °C for 36 h, followed by second heating at 1300 °C for 36 h after regrinding and repelletising. In order to attain a better homogeneity, the products obtained after second heating were reground, pelletised and heated at 1400 °C for 48 h, which was the final annealing temperature for all the samples. The heating and cooling were performed in static air at the rate of 2 deg/min in all the three heating steps. The XRD patterns were recorded on a Philips X-ray diffractometer (Model PW 1710) with monochromatized Cu-Kα radiation. Silicon was used as an external standard for calibration of the instrument. The XRD patterns were well analyzed by comparing with the reported ones. In order to determine the solubility limits, the lattice parameters were refined by a least squares method.

3. Results and discussion

The following sections discuss the results observed in this study. First the binary systems are explained followed by ternary systems.

3.1. $Ce_{1-x}Dy_xO_{2-x/2}$ system

One of the end members, CeO_2, is F-type (Fluorite-type cubic, space group: Fm3m), whereas the other end member, Dy_2O_3, is C-type (C-type cubic, space group: Ia-3). Various phases observed in this particular phase relation are listed in Table 1. As 5 mol % $DyO_{1.5}$ is doped in CeO_2, it gets solubilized thus retaining the parent F-type lattice of CeO_2. This trend is observed till 30 mol% of $DyO_{1.5}$, i.e. a fluorite type solid solution is obtained from nominal composition $Ce_{0.95}Dy_{0.05}O_{1.975}$ to $Ce_{0.70}Dy_{0.30}O_{1.85}$. Beyond that, i.e. from 40 mol% $DyO_{1.5}$, interestingly some small superstructure peaks start appearing, which on careful analysis showed the presence of a C-type ordered structure. These peaks increase in intensity from 40 mol% up to 95 mol% of $DyO_{1.5}$ into CeO_2. It has been reported that at temperatures below 2000 °C, RE_2O_3 (RE = rare-earths) have been found to exist in three types of polymorphs, designated as A (hexagonal), B (monoclinic) and C (cubic) [15] depending upon the rare-earth ionic size and in general on going from La to Lu, the structure of RE_2O_3 changes from A-type to B-type and finally to C-type. Foex and Traverse [16] have reported that the stability of C-type modification increases on decreasing the RE^{3+} ionic size. Dy_2O_3 is known to undergo a phase transition from C-type cubic to monoclinic modification i.e., the B-type at about 1800 °C. The C-type to monoclinic transition temperature for Gd_2O_3 is 1200 °C and in the previous study substitution of ceria into gadolinia could stabilize the C-type modification up to much higher temperatures. This has been explained in detail in the previous work [13]. In CeO_2–$DyO_{1.5}$ system, the transition temperature is higher than those employed in the present study.

Table 1
Phase analysis and lattice parameters of the phases in $Ce_{1-x}Dy_xO_{2-x/2}$ system.

S. no.	Nominal composition	Phase(s)	a (Å)	$a/2$ (of C-type phases)
1	CeO_2	F	5.411(1)	–
2	$Ce_{0.90}Dy_{0.10}O_{1.95}$	F	5.412(3)	–
3	$Ce_{0.85}Dy_{0.15}O_{1.925}$	F	5.413(1)	–
4	$Ce_{0.80}Dy_{0.20}O_{1.90}$	F	5.415(1)	–
5	$Ce_{0.70}Dy_{0.30}O_{1.85}$	F	5.416(1)	–
6	$Ce_{0.60}Dy_{0.40}O_{1.80}$	C	10.829(8)	5.415
7	$Ce_{0.50}Dy_{0.50}O_{1.75}$	C	10.817(8)	5.409
8	$Ce_{0.40}Dy_{0.60}O_{1.70}$	C	10.780(6)	5.390
9	$Ce_{0.30}Dy_{0.70}O_{1.65}$	C	10.752(1)	5.376
10	$Ce_{0.20}Dy_{0.80}O_{1.60}$	C	10.71(1)	5.355
11	$Ce_{0.15}Dy_{0.85}O_{1.575}$	C	10.69(1)	5.345
12	$Ce_{0.10}Dy_{0.90}O_{1.55}$	C	10.689(6)	5.344
13	$Ce_{0.05}Dy_{0.95}O_{1.525}$	C	10.671(1)	5.336
14	$DyO_{1.5}$	C	10.66(1)	5.33

F: Fluorite-type cubic; C: C-type cubic.

Hence, from XRD data, it can be concluded that this system is characterized by the presence of only two phase fields, namely F-type cubic from CeO_2 to $Ce_{0.70}Dy_{0.30}O_{1.85}$ and C-type cubic from $Ce_{0.60}Dy_{0.40}O_{1.80}$ to $Ce_{0.05}Dy_{0.95}O_{1.525}$. As $DyO_{1.5}$ is substituted into CeO_2, the oxygen vacancies are created and these vacancies are the driving force for ordering thus resulting into a C-type ordered lattice. These solid solutions possess anion rich C-type lattice. The bar diagram in Fig. 1(a) depicts the phase fields in this system. The structural analysis of anion-rich Gd_2O_3 (C-type) i.e., $Gd_{1-x}Ce_xO_{1.5+x/2}$ (x = 0.20 and 0.40) was reported [17]. These are isostructural with C-type rare earth oxides, with excess anions required for charge balance. They have body centered

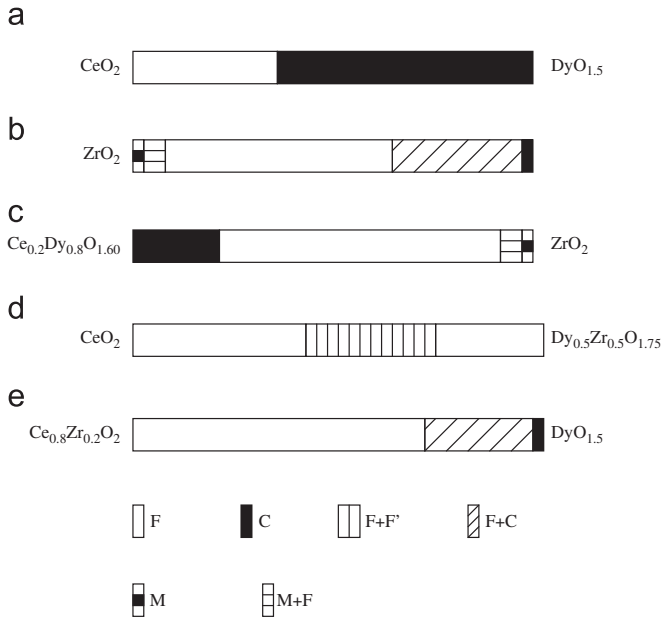

Fig. 1. Bar diagram representing phase relations in (a) CeO_2–$DyO_{1.5}$ series, (b) ZrO_2–$DyO_{1.5}$ series, (c) ZrO_2–$(Ce_{0.20}Dy_{0.80})O_{1.60}$ series, (d) CeO_2–$(Dy_{0.50}Zr_{0.50})O_{1.75}$ series and (e) $DyO_{1.5}$–$(Ce_{0.80}Zr_{0.20})O_2$ series.

cubic lattice (space group Ia-3, No. 206, $Z=32$). The structural analysis reveals them to have two different kinds of metal ion sites, namely 8*b* and 24*d* and two different kinds of anion sites namely 48*e* and 16*c*. Anion-rich C-type dysprosia is also anticipated to have similar structure.

The XRD patterns of various nominal compositions were refined to obtain the lattice parameters and it may be seen from Table 1 that the cell parameters in F-type region increases slightly as a function of Dy^{3+} content whereas it is found to decrease continuously in C-type phase field. The lattice parameter of the nominal compositions $Ce_{0.95}Dy_{0.05}O_{1.975}$–$Ce_{0.70}Dy_{0.30}O_{1.85}$ (F-type solid solutions) increases slightly from 5.412 to 5.416 Å on incorporation of Dy^{3+}. This can be attributed to the relative ionic sizes of Ce^{4+} (0.90 Å) and Dy^{3+} (0. 94 Å) [18]. (The ionic sizes are mentioned for the respective ions in 8-fold co-ordination (in conformity with fluorite-type lattice) throughout the manuscript for maintaining a uniform standard for comparison.) As more and more Dy^{3+} is substituted into CeO_2, lattice parameter increases, as the average cationic radius increases on account of larger size of Dy^{3+} as compared to Ce^{4+}. Likewise, it is expected that the lattice parameter for C-type solid solution (which is observed from nominal composition $Ce_{0.60}Gd_{0.40}O_{1.80}$ onwards) should increase on increasing Dy^{3+} content or vice versa it should decrease as more and more Ce^{4+} is substituted into the Dy_2O_3 lattice. However, the lattice parameter of the C-type solid solution decreases on increasing the Dy^{3+} content. It can plausibly be attributed to the two competing factors that are operating in case of an aliovalent substitution and are explained as follows. When Ce^{4+} is substituted into $DyO_{1.5}$, excess anions are also introduced in the C-type lattice for charge neutralization. As more and more Ce^{4+} is doped in Dy_2O_3 lattice, the average ionic radii decreases (which favors compression of unit cell) whereas ionic repulsion between the excess anions increases (which favors the dilation of the unit cell). The decrease in lattice parameter of the C-type solid solution with decrease in Ce^{4+} content (or with increase in Dy^{3+} content) can thus be attributed to the predominance of repulsion factor over the relative ionic sizes. A similar trend was observed in CeO_2–Gd_2O_3 series as well, wherein the lattice parameter of C-type solid solution decreased on increasing the Gd^{3+} content [19]. Also, on comparing CeO_2–Dy_2O_3 series with the CeO_2–Gd_2O_3 series, it is worth noting that the ionic size difference between Dy^{3+} (0.94 Å) and Ce^{4+} (0.90 Å) is much less than as compared to that between Gd^{3+} (0.98 Å) and Ce^{4+} (0.90 Å). This difference leads to very interesting manifestation in the trend observed in the lattice parameters of F- and C-type solid solutions observed in CeO_2–$GdO_{1.5}$ [19] and CeO_2–$DyO_{1.5}$ series. There is a steeper increase in lattice parameter of F-type solid solution in CeO_2–$GdO_{1.5}$ as compared to the CeO_2–$DyO_{1.5}$ series whereas the lattice parameter of the C-type solid solution in the system CeO_2–$GdO_{1.5}$ shows smaller variation than in CeO_2–$DyO_{1.5}$ system. Fig. 2 gives the variation of lattice parameter of $Ce_{1-x}Dy_xO_{2-x/2}$ solid solution with mol% Dy^{3+} (for the sake of comparison, the lattice parameters of the C-type solid solutions have been halved).

3.2. $Zr_{1-x}Dy_xO_{2-x/2}$ system

Table 2 elaborates on the phases observed in $Zr_{1-x}Dy_xO_{2-x/2}$ system and the lattice parameters obtained by refinement of their respective XRD data. Powder XRD patterns reveal that one of the end members, ZrO_2 is monoclinic and Dy_2O_3 (as mentioned above) is cubic (C-type). The careful observation of XRD patterns of the nominal compositions $Zr_{0.975}Dy_{0.025}O_{1.988}$, $Zr_{0.95}Dy_{0.05}O_{1.975}$ and $Zr_{0.90}Dy_{0.10}O_{1.95}$, showed them to be biphasic consisting of fluorite-type phase along with monoclinic phase (Table 2), with concomitant reduction in the peak intensity of monoclinic zirconia with increase in Dy^{3+} content. The peaks corresponding

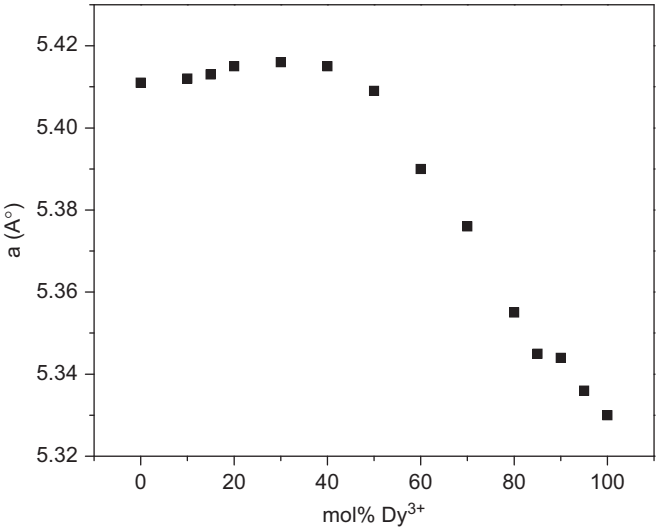

Fig. 2. Lattice parameter variation $Ce_{1-x}Dy_xO_{2-x/2}$ series with mol% Dy^{3+}.

Table 2
Phase analysis and lattice parameters of the phases in $Zr_{1-x}Dy_xO_{2-x/2}$ system.

S. no.	Nominal composition	Phase (s)	a (Å)
1	$DyO_{1.5}$	C	10.66(1)
2	$Zr_{0.10}Dy_{0.90}O_{1.55}$	C	10.622(4)
		F	5.309(2)
3	$Zr_{0.20}Dy_{0.80}O_{1.60}$	C	10.596(3)
		F	5.258(3)
4	$Zr_{0.30}Dy_{0.70}O_{1.65}$	F	5.257(1)
		C	10.55(1)
5	$Zr_{0.35}Dy_{0.65}O_{1.675}$	F	5.272(5)
		C	[a]
6	$Zr_{0.40}Dy_{0.60}O_{1.70}$	F	5.244(1)
7	$Zr_{0.50}Dy_{0.50}O_{1.75}$	F	5.241(1)
8	$Zr_{0.60}Dy_{0.40}O_{1.80}$	F	5.195(4)
9	$Zr_{0.70}Dy_{0.30}O_{1.85}$	F	5.166(1)
10	$Zr_{0.80}Dy_{0.20}O_{1.90}$	F	5.144(3)
11	$Zr_{0.85}Dy_{0.15}O_{1.925}$	F	5.149(1)
12	$Zr_{0.90}Dy_{0.10}O_{1.95}$	F	5.143(1)
		M	[a]
13	$Zr_{0.95}Dy_{0.05}O_{1.975}$	F	5.136(5)
		M	$a=5.329(10)$, $b=5.16(1)$, $c=5.157(7)$, $\beta=99.0°(2)$
14	$Zr_{0.975}Dy_{0.025}O_{1.988}$	M	$a=5.339(6)$, $b=5.217(8)$, $c=5.165(4)$, $\beta=99.2°(1)$
		F	[a]
15	ZrO_2	M	$a=5.313(1)$, $b=5.212(1)$, $c=5.147(1)$, $\beta=99.22°(1)$

F: Fluorite-type cubic; C: C-type cubic; M: Monoclinic.
[a] Negligible intensity and hence not refined.

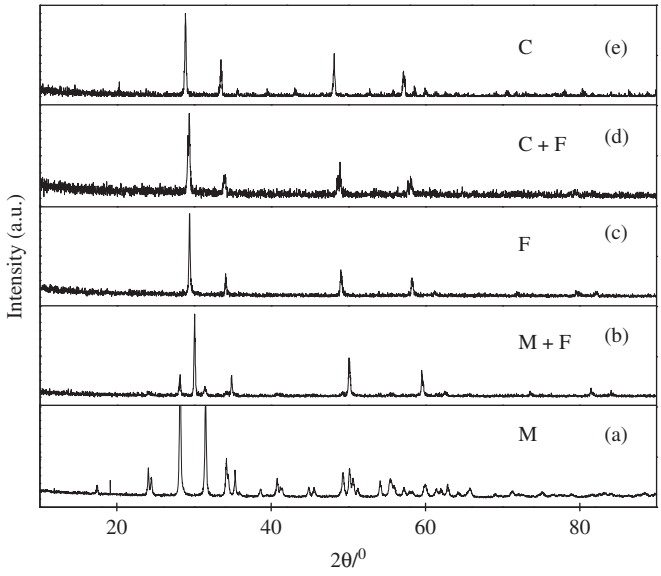

Fig. 3. XRD patterns in $Zr_{1-x}Dy_xO_{2-x/2}$ series: (a) ZrO_2; (b) $Zr_{0.90}Dy_{0.10}O_{1.95}$; (c) $Zr_{0.50}Dy_{0.50}O_{1.75}$; (d) $Zr_{0.30}Dy_{0.70}O_{1.65}$; (e) Dy_2O_3.

to m-ZrO_2, subsequently disappeared and the next composition, $Zr_{0.85}Dy_{0.15}O_{1.925}$ was found to be fully stabilized cubic zirconia. Therefore, it can be inferred that about 12.5 mol % $DyO_{1.5}$ i.e., the average between $Zr_{0.90}Dy_{0.10}O_{1.95}$ (biphasic) and $Zr_{0.85}Dy_{0.15}O_{1.925}$ (monophasic) can fully stabilize the cubic zirconia under the experimental conditions employed in this investigation. The stabilized fluorite-type phase exists up to the nominal composition $Zr_{0.40}Dy_{0.60}O_{1.70}$. There is an increase in lattice parameter of the fluorite-type phase i.e., the stabilized zirconia, from 5.136(5) to 5.244(1) Å because of the substitution of smaller ion (Zr^{4+}) by the bigger ion (Dy^{3+}) on going from $Zr_{0.95}Dy_{0.05}O_{1.975}$ to $Zr_{0.40}Dy_{0.60}O_{1.70}$. This indicates the presence of a wide homogeneity range of dysprosia-stabilized-zirconia. The peaks due to C-type dysprosia started appearing from the nominal composition $Zr_{0.35}Dy_{0.65}O_{1.85}$ onwards and a biphasic region consisting of stabilized fluorite-type phase coexisting with C-type phase is observed till the nominal composition $Zr_{0.10}Dy_{0.90}O_{1.55}$. Fig. 3 depicts typical XRD patterns belonging to this series. Fig. 1(b) shows the phase fields observed in this system. The larger difference in ionic sizes and the structures of zirconia and dysprosia as compared to ceria and dysprosia can account for existence of biphasicity in $Zr_{1-x}Dy_xO_{2-x/2}$ whereas $Ce_{1-x}Dy_xO_{2-x/2}$ was observed to be single-phasic throughout.

3.3. $Zr_{1-x}(Ce_{0.2}Dy_{0.8})_xO_{2-0.4x}$ system

In this series, one of the end members $Ce_{0.2}Dy_{0.8}O_{1.60}$ is C-type cubic. On substituting 10 mol% ZrO_2 (which is monoclinic at room temperature), i.e. the nominal composition $Zr_{0.10}Ce_{0.18}Dy_{0.72}O_{1.64}$, the C-type cubic lattice is retained. The lattice parameter of the resultant solid solution is slightly lower than the end member $Ce_{0.2}Dy_{0.8}O_{1.60}$. The average cationic size of $Ce_{0.2}Dy_{0.8}O_{1.60}$ is 0.93 Å which is more than Zr^{4+} (0.75 Å) and hence the decrease in cell parameter can be explained using average ionic size considerations. The trend is continued in the nominal compositions $Zr_{0.15}Ce_{0.17}Dy_{0.68}O_{1.66}$ and $Zr_{0.20}Ce_{0.16}Dy_{0.64}O_{1.68}$, containing 15 mol % and 20 mol % ZrO_2 substitution, respectively, thus retaining the C-type lattice with concomitantly decreasing lattice parameters. The nominal compositions from $Zr_{0.30}Ce_{0.14}Dy_{0.56}O_{1.72}$ to $Zr_{0.80}Ce_{0.04}Dy_{0.16}O_{1.92}$, exhibit an F-type phase. This can be explained as follows. For every Zr^{4+} that is introduced into the lattice in place of ($Ce_{0.2}Dy_{0.8}$) cation, 0.4 excess oxygen anions are also added into the lattice to maintain electroneutrality. The C-type lattice in $REO_{1.5}$ is manifested due to the ordering of 0.5 oxygen ion vacancy. Till 20 mol% of Zr^{4+} doping, the excess anions do not affect the ordering but beyond that, the excess anions disrupt the ordering of C-type structure and it gradually transforms to F-type lattice. Thereafter, the solubility of ZrO_2 in $Ce_{0.2}Dy_{0.8}O_{1.60}$ saturates and $Zr_{0.85}Ce_{0.03}Dy_{0.12}O_{1.94}$ (85 mol% ZrO_2) onwards, excess ZrO_2 is phase separated from the lattice and in turn monoclinic zirconia peaks also appear along with the F-type phase. Therefore, the nominal compositions $Zr_{0.85}Ce_{0.03}Dy_{0.12}O_{1.94}$ and $Zr_{0.90}Ce_{0.02}Dy_{0.08}O_{1.96}$, exhibit a biphasic phase field consisting of a monoclinic phase and an F-type phase. The phase relations observed in this system are exhibited by the bar diagram in Fig. 1(c). Fig. 4 shows the representative XRD patterns depicting the phase trends in this series. Table 3 gives

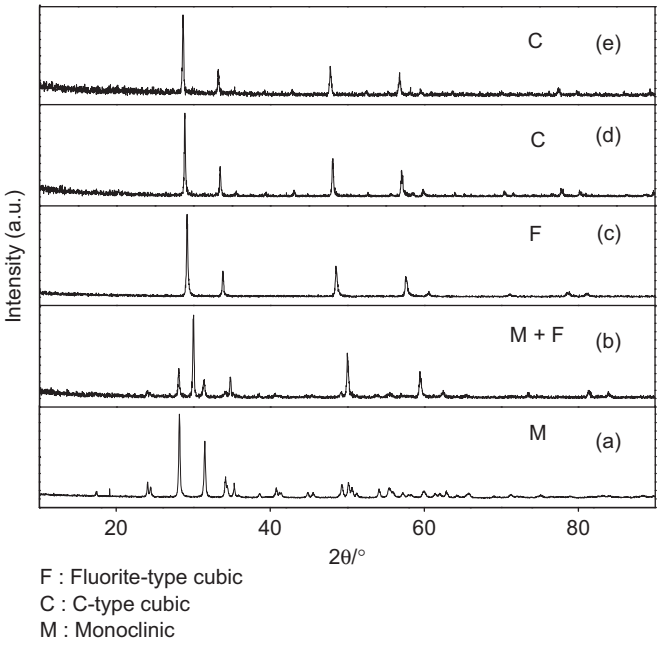

Fig. 4. XRD Patterns in $Zr_{1-x}(Ce_{0.2}Dy_{0.8})_xO_{2-0.4x}$ series: (a) ZrO_2 ;(b) $Zr_{0.90}Ce_{0.02}Dy_{0.08}O_{1.96}$; (c) $Zr_{0.30}Ce_{0.14}Dy_{0.56}O_{1.72}$; (d) $Zr_{0.10}Ce_{0.18}Dy_{0.72}O_{1.64}$; (e) $Ce_{0.2}Dy_{0.8}O_{1.60}$.

Table 3
Phase analysis and lattice parameters of the products in $Zr_{1-x}(Ce_{0.2}Dy_{0.8})_xO_{2-0.4x}$ system.

S. No.	Nominal composition	Phase analysis	a (Å)
1	$Zr_{0.00}Ce_{0.2}Dy_{0.80}O_{1.60}$	C	10.70(1)
3	$Zr_{0.10}Ce_{0.18}Dy_{0.72}O_{1.64}$	C	10.677(3)
4	$Zr_{0.15}Ce_{0.17}Dy_{0.68}O_{1.66}$	C	10.665(2)
5	$Zr_{0.20}Ce_{0.16}Dy_{0.64}O_{1.68}$	C	10.649(2)
6	$Zr_{0.30}Ce_{0.14}Dy_{0.56}O_{1.72}$	F	5.304(2)
7	$Zr_{0.40}Ce_{0.12}Dy_{0.48}O_{1.76}$	F	5.274(1)
8	$Zr_{0.50}Ce_{0.10}Dy_{0.40}O_{1.80}$	F	5.243(1)
9	$Zr_{0.60}Ce_{0.08}Dy_{0.32}O_{1.84}$	F	5.212(1)
10	$Zr_{0.70}Ce_{0.06}Dy_{0.24}O_{1.88}$	F	5.184(1)
11	$Zr_{0.80}Ce_{0.04}Dy_{0.16}O_{1.92}$	F	5.170(2)
12	$Zr_{0.85}Ce_{0.03}Dy_{0.12}O_{1.94}$	M	[a]
		F	5.156(1)
13	$Zr_{0.90}Ce_{0.02}Dy_{0.08}O_{1.96}$	M	a=5.312(6), b=5.236(7), c=5.158(5), β=99.0°(2)
		F	5.152(1)
14	$Zr_{0.95}Ce_{0.01}Dy_{0.04}O_{1.98}$	M	a=5.332(9), b=5.199(9), c=5.171(4), β=99.1°(2)
		F	5.148(1)
15	ZrO_2	M	a=5.313(1),b=5.212(1),c =5.147(1),β=99.22° (1)

F: F-type cubic; C: C-type cubic; M: Monoclinic.
[a] Negligible intensity and hence not refined.

the refined lattice parameters of various nominal compositions belonging to the $Zr_{1-x}(Ce_{0.2}Dy_{0.8})_xO_{2-0.4x}$ system. The lattice parameter of the F-type phase decreases on increasing ZrO_2 content due to decrease in average ionic radii.

Table 4
Phase analysis and lattice parameters of the products in $(Dy_{0.5}Zr_{0.5})_{1-x}Ce_xO_{1.75+x/4}$ system.

S. no.	Nominal composition	Phase analysis	a (Å)
1	$Dy_{0.5}Zr_{0.5}Ce_{0.00}O_{1.75}$	F	5.241(1)
2	$Dy_{0.475}Zr_{0.475}Ce_{0.05}O_{1.763}$	F	5.245(1)
3	$Dy_{0.45}Zr_{0.45}Ce_{0.10}O_{1.775}$	F	5.265(2)
4	$Dy_{0.425}Zr_{0.425}Ce_{0.15}O_{1.788}$	F	5.271(1)
5	$Dy_{0.40}Zr_{0.40}Ce_{0.20}O_{1.80}$	F	5.283(1)
		F′	[a]
6	$Dy_{0.35}Zr_{0.35}Ce_{0.30}O_{1.825}$	F	5.371(1)
		F′	[a]
7	$Dy_{0.30}Zr_{0.30}Ce_{0.40}O_{1.85}$	F	5.334(2)
		F′	[a]
8	$Dy_{0.25}Zr_{0.25}Ce_{0.50}O_{1.875}$	F	5.349(3)
		F′	[a]
9	$Dy_{0.20}Zr_{0.20}Ce_{0.60}O_{1.90}$	F	5.358(1)
10	$Dy_{0.10}Zr_{0.10}$ $Ce_{0.80}O_{1.95}$	F	5.380(1)
11	$Dy_{0.05}Zr_{0.05}Ce_{0.90}O_{1.975}$	F	5.399(1)
12	$Dy_{0.025}Zr_{0.025}Ce_{0.95}O_{1.988}$	F	5.407(1)
13	CeO_2	F	5.411(1)

F, F′: Fluorite-type cubic.
[a] Unidentified phase (presumably fluorite type).

3.4. $(Dy_{0.5}Zr_{0.5})_{1-x}Ce_xO_{1.75+x/4}$

Both the end members in this series have F-type (fluorite-type) lattice. Table 4 elaborates on various phase fields present in the given system and their corresponding lattice parameters. One of the end members of this series is $Dy_{0.5}Zr_{0.5}O_{1.75}$, which has a defect fluorite lattice. The nominal composition $Dy_{0.475}Zr_{0.475}Ce_{0.05}O_{1.763}$ wherein 5 mol% of CeO_2 was doped in $Dy_{0.5}Zr_{0.5}O_{1.75}$ was found to be F-type cubic. The trend continued till the nominal composition $Dy_{0.425}Zr_{0.425}Ce_{0.15}O_{1.788}$ and the lattice parameter increases from 5.245 Å in $Dy_{0.475}Zr_{0.475}Ce_{0.05}O_{1.763}$ to 5.271 Å in $Dy_{0.425}Zr_{0.425}Ce_{0.15}O_{1.788}$. This can be explained on the basis of increase in average cationic radius on doping ceria. Beyond that, few compositions, $((Dy_{0.5}Zr_{0.5})_{1-x}Ce_xO_{1.75+x/4}$; x=0.2 to 0.5) were found to have broad peaks in their XRD patterns, which showed the presence of a F-type lattice with another unidentified lattice, presumably another F-type lattice. The presence of C-type phase is ruled out because of two reasons. The phase field is flanked on both the sides by F-type phases and hence presence of two F-type phases in this intermediate region is more probable. In addition, the absence of any superstructure peaks negates the presence of C-type ordering. The refinement of the XRD data for the major fluorite phase gave the lattice parameters, which increase with increase in ceria content. Thereafter, the compositions $Dy_{0.20}Zr_{0.2}Ce_{0.60}O_{1.90}$–$Dy_{0.025}Zr_{0.025}Ce_{0.95}O_{1.988}$ were found to be single phasic F-type for which the lattice parameter increases from 5.358 Å to 5.407 Å, which could be attributed based on the increase in average cationic size in these compositions. Fig. 1(d) depicts various phase fields observed for this system.

3.5. $Dy_{1-x}(Ce_{0.8}Zr_{0.2})_xO_{1.5+x/2}$ system

The phase analysis and the refined lattice parameters of the observed phases for this particular series are depicted in

Table 5. The end member, $Ce_{0.8}Zr_{0.2}O_2$, is F-type cubic in nature. As 5 mol% $DyO_{1.5}$ is doped in $Ce_{0.8}Zr_{0.2}O_2$, i.e. in the nominal composition $Ce_{0.76}Zr_{0.19}Dy_{0.05}O_{1.975}$, the F-type lattice is retained. In fact, $Ce_{0.8}Zr_{0.2}O_2$ parent lattice can solubilize up to 60 mol% $DyO_{1.5}$ thus retaining fluorite-type lattice. Thus, a wide solubility range of fluorite-type phase field is observed from $Ce_{0.76}Zr_{0.19}Dy_{0.05}O_{1.975}$ to $Ce_{0.32}Zr_{0.08}Dy_{0.60}O_{1.70}$. An interesting trend was observed in the lattice parameter of fluorite-type solid solution in this range. The average cationic radius of $Ce_{0.8}Zr_{0.2}O_2$ is 0.87 Å whereas the radius of Dy^{3+} is 0.94 Å. Thus despite the fact that a smaller cation is being replaced by a larger cation with increase in the content of Dy^{3+}, the lattice parameter shows a continuous decrease which can be explained based on the predominance of oxygen vacancies (incorporated due to Dy^{3+} substitution) factor over the average cationic radius. Beyond that, the nominal composition, $Ce_{0.24}Zr_{0.06}Dy_{0.70}O_{1.65}$, shows the appearance of another phase along with the existing fluorite-type phase. The new phase appears to have fluorite-type symmetry and a biphasic phase field comprising of probably two fluorite type phases is obtained. However when X-ray diffraction data was collected for the nominal composition $Ce_{0.12}Zr_{0.03}Dy_{0.85}O_{1.575}$ for a longer duration, small peaks corresponding to C-type lattice were observed (Fig. 5), which implies that the biphasic field consists of an F-type and a C-type phase rather that two fluorite-type phases. This conclusion seems plausible in view of the fact that these compositions have high $DyO_{1.5}$ content which has a C-type structure. The lattice parameters of the second phase are refined based on fluorite-type lattice since the superstructure peaks for C-type ordering are very weak. The phase evolution in this series is well depicted in Fig. 6. Various phase fields observed in this system are well depicted in Fig. 1(e).

Table 5
Phase analysis and lattice parameters of the phases in $(Ce_{0.8}Zr_{0.2})_{1-x}Dy_xO_{2-x/2}$ system.

S. no.	Nominal composition	Phase analysis	a (Å)
1	$Ce_{0.76}Zr_{0.19}Dy_{0.05}O_{1.975}$	F	5.406(1)
2	$Ce_{0.72}Zr_{0.18}Dy_{0.10}O_{1.95}$	F	5.396(1)
3	$Ce_{0.68}Zr_{0.17}Dy_{0.15}O_{1.925}$	F	5.377(1)
4	$Ce_{0.64}Zr_{0.16}Dy_{0.20}O_{1.90}$	F	5.365(3)
5	$Ce_{0.56}Zr_{0.14}Dy_{0.30}O_{1.85}$	F	5.317(1)
6	$Ce_{0.48}Zr_{0.12}Dy_{0.40}O_{1.80}$	F	5.298(2)
7	$Ce_{0.40}Zr_{0.10}Dy_{0.50}O_{1.75}$	F	5.240(1)
8	$Ce_{0.32}Zr_{0.08}Dy_{0.60}O_{1.70}$	F	5.268(1)
9	$Ce_{0.24}Zr_{0.06}Dy_{0.70}O_{1.65}$	F	5.221(2)
		C	[a]
10	$Ce_{0.16}Zr_{0.04}Dy_{0.80}O_{1.60}$	F	5.210(2)
		C	5.155(8)
11	$Ce_{0.12}Zr_{0.03}Dy_{0.85}O_{1.575}$	F	5.196(2)
		C	5.148(8)
12	$DyO_{1.5}$	C	10.66(1)

F, F′: Fluorite-type cubic; C: C-type cubic.
C-type phase refined on F-type lattice because of very low intensity of superstructure peaks.
[a] Unidentified phase (presumably C-type).

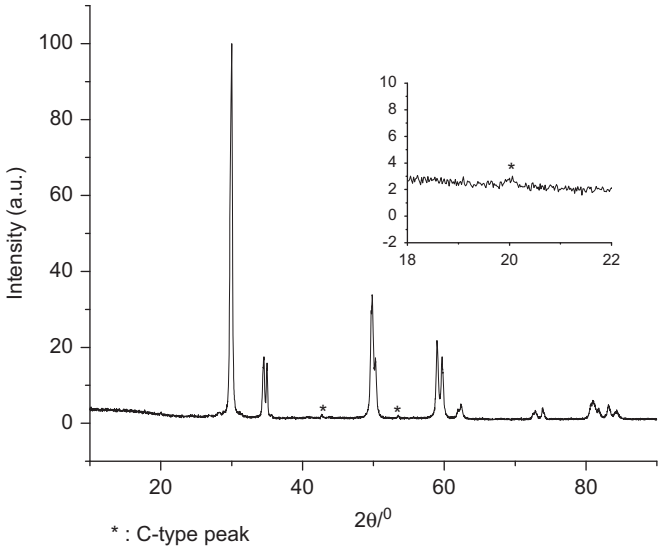

Fig. 5. XRD pattern of nominal composition $Ce_{0.12}Zr_{0.03}Dy_{0.85}O_{1.575}$ showing the appearance of C-type peaks.

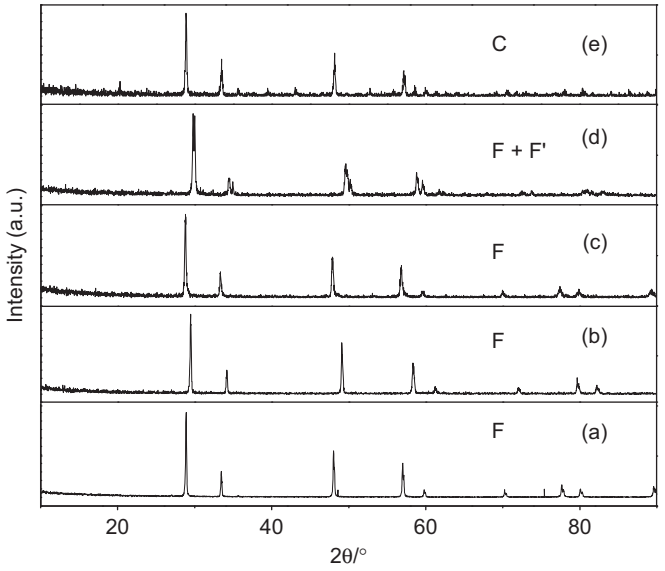

Fig. 6. XRD patterns in $Dy_{1-x}(Ce_{0.8}Zr_{0.2})_xO_{1.5+x/2}$ series: (a) $Ce_{0.80}Zr_{0.20}O_2$; (b) $Ce_{0.76}Zr_{0.19}Dy_{0.05}O_{1.975}$; (c) $Ce_{0.68}Zr_{0.17}Dy_{0.15}O_{1.925}$; (d) $Ce_{0.16}Zr_{0.04}Dy_{0.80}O_{1.60}$; (e) Dy_2O_3.

The ternary phase relations in CeO_2–$DyO_{1.5}$–ZrO_2 are shown in Fig. 7. On comparing it with the previous systems like CeO_2–Gd_2O_3–ThO_2 [14], it was observed that the cubic phase field supported by CeO_2–Gd_2O_3–ThO_2 is much wider as compared to the present system. This can be explained on the basis of the cubic nature of all the reactants in CeO_2–Gd_2O_3–ThO_2 system thus ensuring more miscibility and hence a wider cubic phase field. In present system, one of the reactants zirconia, has got monoclinic structure. And this also accounts for more number of phase fields in the present system as compared to CeO_2–Gd_2O_3–ThO_2 ternary system.

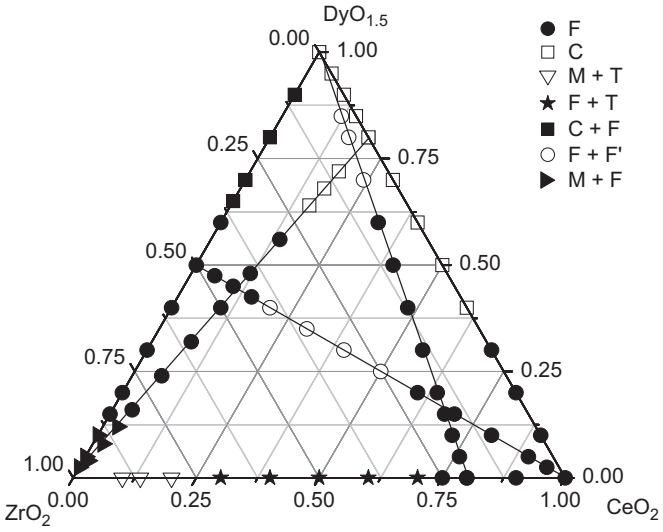

Fig. 7. Ternary phase relation in CeO_2–$DyO_{1.5}$–ZrO_2 system.

4. Conclusions

The sub-solidus ternary phase relation in CeO_2–$DyO_{1.5}$–ZrO_2 was established as a result of this study for the first time to the best of our knowledge. The detailed phase relation studies in this ternary system (Fig. 7) revealed several interesting features. A wide range of cubic phase field could be observed in this ternary system. Dysprosia was able to stabilize cubic zirconia under the given experimental conditions. The trends in lattice parameters in anion-excess C-type phases were observed to be the function of two competing factors i.e. average cationic size and repulsion between excess anions and it was usually the repulsion factor which was found to predominate. A wide solubility of both Dy_2O_3 (burnable poison) and ZrO_2 (host lattice) could be observed in ceria (surrogate for plutonia). This is a significant result from the point of view of the viability of given system as inert matrix fuel. In addition, several single phasic fluorite-type phases could also be explored for superior ionic conductivity.

References

[1] C. Lombardi, A. Mazzola, Exploiting the plutonium stockpiles in PWRs by using inert matrix fuel, Annals of Nuclear Energy 23 (1996) 1117–1126.
[2] M. Burghartz, H. Matzke, C. Leger, G. Vambenepe, M. Rome, Inert matrices for transmutation of actinides: fabrication, thermal properties and radiation stability of ceramic materials, Journal of Alloys and Compounds 544 (1998) 271–273.
[3] C. Degueldre, J.M. Paratte, Concepts for an inert matrix fuel, an overview, Journal of Nuclear Materials 274 (1999) 1–6.
[4] K. Bakker, Hj. Hein, R.J.M. Konings, R.R. van der Laan, H. Matzke, P. Van Vlaanderen, Thermophysical property measurement and ion implantation studies on $CePO_4$, Journal of Nuclear Materials 252 (1998) 228–234.
[5] N. Sasajima, T. Matsui, K. Hojou, S. Furuno, H. Otsu, K. Izui, T. Muromura, Radiation damage in yttria stabilized zirconia under Xe irradiation, Nuclear Instruments and Methods in Physics Research B 141 (1998) 487–493.
[6] K.E. Sickafus, Hj. Matzke, K. Yasuda, P. Chodak III, R.A. Verrall, P. G. Lucuta, R.H. Andrews, A. Turos, R. Fromknecht, N.P. Baker, Radiation damage effects in cubic-stabilized zirconia irradiated with 72 MeV I^+ ions, Nuclear Instruments and Methods in Physics Research B 141 (1998) 358–365.
[7] A.K. Tyagi, B.R. Ambekar, M.D. Mathews, Simulation of lattice thermal expansion behaviour of $Th_{1-x}Pu_xO_2$ ($0.0 \le x \le 1.0$) using CeO_2 as a surrogate material for PuO_2, Journal of Alloys and Compounds 337 (2002) 277–281.
[8] A. Rouanet, Zirconium dioxide–Lanthanide oxide system close to the melting point, Revue Internationale des Hautes Températures et des Réfractaires 8 (1971) 161–180.
[9] P. Duwez, F. Odell, Phase relationships in the system Zirconia-Ceria, Journal of the American Ceramic Society 33 (1950) 280.
[10] D.H. Lee, S.K. Cho, C.H. Yo, K.H. Kim, S.H. Park, Electrical conductivity of solid solution $x CeO_2 + (_{1-x})Dy_2O_3$; $0.01 \le x \le 0.10$, Materials Chemistry and Physics 37 (1994) 17–22.
[11] Y. Wang, T. Mori, J. Li, J. Drennan, Synthesis, characterization and electrical conduction of 10 mol% Dy_2O_3 doped ceria ceramics, Journal of the European Ceramic Society 25 (2005) 949–956.
[12] V. Grover, A.K. Tyagi, Sub-solidus phase equilibria in the CeO_2–ThO_2–ZrO_2 system, Journal of Nuclear Materials 305 (2002) 83–89.
[13] V. Grover, A.K. Tyagi, Phase relation studies in CeO_2–Gd_2O_3–ZrO_2 system, Journal of Solid State Chemistry 177 (2004) 4197–4204.
[14] V. Grover, A.K. Tyagi, Investigations of ternary phase relations in a CeO2–Gd_2O_3–ThO_2 system, Journal of the American Ceramic Society 89 (2006) 2917–2921.
[15] G. Adachi, N. Imanaka, The binary rare earth oxides, Chemical Reviews 98 (1998) 1479–1514.
[16] M. Foex, J.P. Traverse, Polymorphism of rare earth sesquioxide at high temperature, Revue Internationale des Hautes Températures et des Réfractaires 3 (1966) 429–453.
[17] V. Grover, S.N. Achary, A.K. Tyagi, Structural analysis of anion-excess C-type rare earth oxides: a case study with $Gd_{1-x}Ce_xO_{1.5+x/2}$.($x = 0.20$ and 0.40), Journal of Applied Crystallography 36 (2003) 1082–1084.
[18] R.D. Shannon, Revised effective ionic radii and systematic studies of interatomic distances in halides and chalcogenides, Acta Crystallographica A 32 (1976) 751–767.
[19] V. Grover, A.K. Tyagi, Phase relations, lattice thermal expansion in CeO_2–Gd_2O_3 system, and stabilization of cubic gadolinia, Materials Research Bulletin 39 (2004) 859–866.